

Robotic Micromanipulation for Active Pin Alignment in Electronic Soldering Industry

Hao Ren, Xinyu Wu, *Member, IEEE*, and Wanfeng Shang

Abstract—In the context of robotic high-precision soldering, we propose an image-based pin alignment control method based on active plastic deformation. The plastic deformation is a well-known failure mechanism in most situations, which includes a phenomenon that the objects do not return original state. Here, in contrast to this convention, we utilize the plastic deformation of the metal pin to do pin alignment for improving the quality of the solder joint. To address this, we embed the springback compensation into the image-based pin alignment controller. Lastly, the proposed strategy is successfully demonstrated and evaluated in a practical modified robotic manipulation system. The result shows that the alignment error is less than $20\mu\text{m}$, which is far less than pin alignment without considering plastic deformation and elastic recovery. This work considers active plastic deformation and spontaneous elastic recovery of soft object, which would greatly promote the use of robotics in micromanufacturing and microfabrication in lab and industry, especially for soft objects.

I. INTRODUCTION

With the growing demands at the microscale, robotics for high-precision manipulation at small scale have attracted more and more attention [1], [2]. Nowadays, this technology has been successfully implemented on various applications, such as microfluid dispensing tasks [3], high-precision gluing tasks [4], high-precision peg-in-hole tasks [5], [6] and accurate alignment tasks in industrial environment [7]. For assembly of small components, some innovative gripper or micro-tweezers have been designed and effectively integrated into a robotic system to pick small objects for precision micrometer and sub-micrometer positioning and orientation control under micro-vision systems [8], [9]. In addition, a micro-hand having two fingers was built using cooperative parallel mechanisms to dexterously rotate sphere components [10]. However, these methods require additional devices and hardware, which alter them used in practical PCB production line. In order to improve the quality and qualified rate of

This work was funded by National Natural Science Foundation of China (Grant No. 62073308), Shenzhen Institute of Artificial Intelligence and Robotics for Society, Key-Area Research and Development Program of Guangdong Province (Grant No. 2020B090925001), and Shenzhen Key Basic Research project (Grant No. JCYJ20200109114827177).

Wanfeng Shang and Xinyu Wu are with CAS Key Laboratory of Human-Machine Intelligence-Synergy Systems, Chinese Academy of Sciences, Shenzhen 518055, China, also with Guangdong Provincial Key Laboratory of Robotics and Intelligent System, Chinese Academy of Sciences, Shenzhen 518055, China, also with Shenzhen Institute of Advanced Technology, Chinese Academy of Sciences, Shenzhen 518055, China (e-mail: wf.shang@siat.ac.cn; xy.wu@siat.ac.cn).

Hao Ren is with Shenzhen Institute of Advanced Technology, Chinese Academy of Sciences, Shenzhen 518055, China, also with University of Chinese Academy of Sciences, Beijing 100000, China (e-mail: hao.ren1@siat.ac.cn).

Corresponding author: Wanfeng Shang(wf.shang@siat.ac.cn)

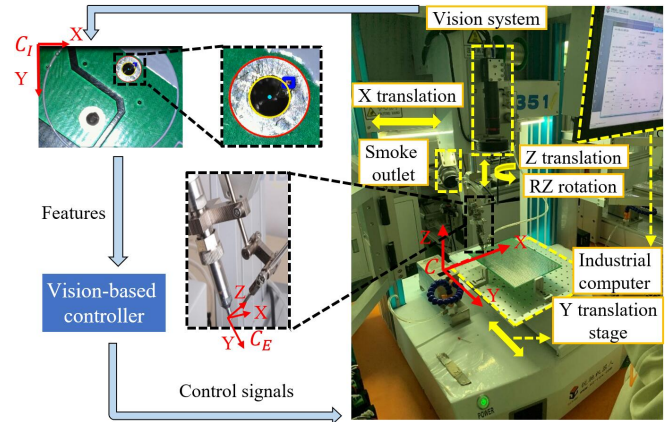


Fig. 1. The micromanipulation system. The manipulation system mainly include a robotic manipulator, a vision system, and an industrial computer.

robotic Through-Hole Technology (THT), researchers have carried out a lot of studies. These issues involved can be divided into two broad categories: one is to explore the influence of lead-free alloys with different components on the performance of solder joints [11]–[13]; the other is to focus on the automatic optical inspection (AOI) process after soldering, aiming to improve the inspection performance of AOI, which is capable of classifying the quality of through-hole (TH) solder joints very precisely [14]. The former basic researches are helpless for soldering defects caused by process problems, while the latter approach is inefficient since it is actually a kind of post-process technology, and thus none of them can deal with external disturbance and system uncertainty online.

In practical automatic soldering production line, the deformation of electronic components' pin often occurs due to the flexibility of the metal pin and the uncertainty disturbance of the components plug-in system. The deformation of the pin causes the pin's free end to deviate from the center of the solder joint, which will increase the risk of bridging with adjacent joints, as shown in Fig. 2(a). Once the distance between the pin and through-hole wall is too small, surface tension and capillary force will lead to insufficient through-hole fill. Fig. 2(b)(1)-(2) shows the uneven solder distribution due to the pin's deformation. (3) and (4) give two representative solder joints, where (3) is a standard solder joint whose pin is completely coincident with the through-hole axis which is the correction result of (1), and (4) is a non-standard but high-quality solder joint which is the correction result of (2). In short, it is necessary to keep the liquid-

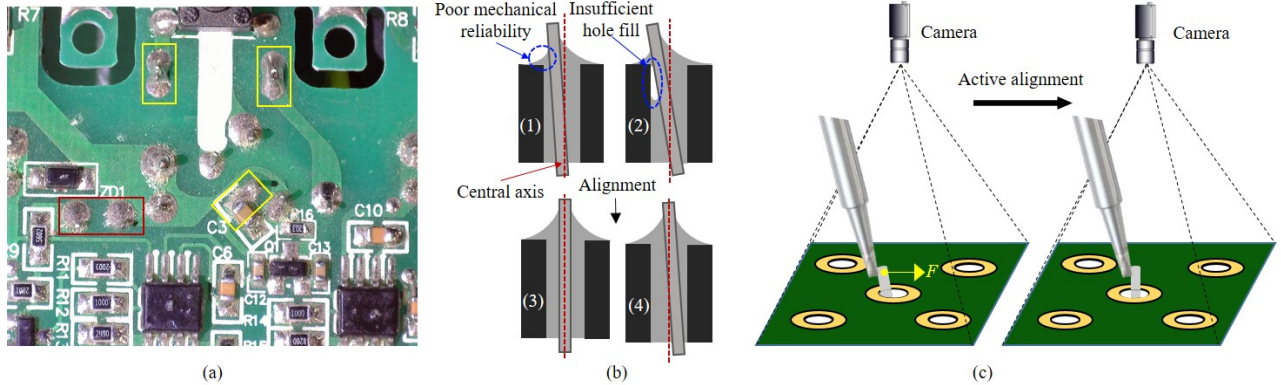


Fig. 2. Soldering problems caused by pin deformation in practical industry environment. (a) An integrated circuit(IC) board produced by an practical automatic soldering line, in which the yellow box indicates the bridging defect, and the red box indicates the solder joint with excessive pin's inclination. (b) Cross sections of four solder joints. (c) Active pin alignment to get a high-quality solder joint.

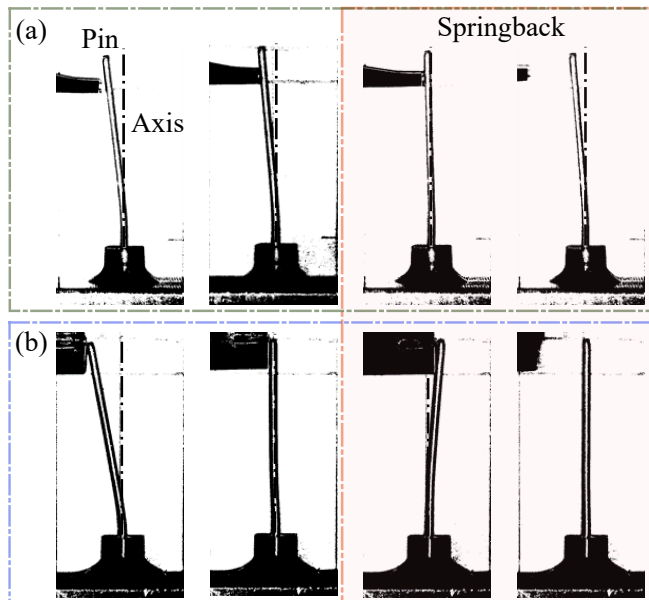


Fig. 3. Springback in pin alignment. (a) The alignment error caused by elastic recovery after unloading the external force. (b) A better result of pin alignment with springback compensation.

solid two-phase interface of solder at the steady state during soldering THC to get a high-quality solder joint.

The base material of modern electronic component pin is Cu or FeNi with flexibility, so in the actual pin alignment operation, we found that after removing the external force, the metal pin will spontaneously carry out elastic recovery movement. If the pin is only moved to the center of the solder joint without considering about springback, the pin will deviate from the desired position due to its own elastic recovery, which will bring visible error to pin alignment as shown in Fig. 3(a). Therefore, it is essential to consider springback compensation when do pin alignment as shown in Fig. 3(b).

In this paper, a typical micromanipulation system as shown in Fig. 1 is used to solve the soldering defects caused by pin deformation of electronic components. Firstly, we analyze

the phenomenon of elastic recovery in the process of metal pin alignment, also do a lot of experiments to determine the compensation for it. Then the image-based visual servoing [15] method is used to precisely control the manipulator to move the pin's free end to the desired position in the image space with considering the pin's springback after removing the external force.

The rest of this paper is organized as follows. Section II briefly introduces the micromanipulation system. Section III introduces a high precise image-based active pin alignment control method with springback compensation. The proposed alignment method is applied into a practical robotic soldering system, which is illustrated in section IV. Finally, this paper is concluded in section V.

II. THE CONFIGURATION OF A TYPICAL MICROMANIPULATION SYSTEM

A typical micromanipulation system is shown in Fig. 1, which is mainly constituted of four parts: an industrial computer, a vision system, a robotic micromanipulator and an integrated temperature controller. And the system often has five coordinate systems: the word coordinate system C_W , the robot base coordinate system C_B , the end coordinate system C_E , the image coordinate system C_I , the object coordinate system C_O .

Especially, ${}^i\boldsymbol{x}$ denotes the vector \boldsymbol{x} expressed in coordinate system C_i (Considering the simplicity of writing, the vector of in the word coordinate system omits the left superscript W). ${}^B\boldsymbol{R}_A$ and ${}^B\boldsymbol{t}_A$ are the rotation matrix and the translation vector from C_A to C_B . So the transformation relationship from C_A to C_B can be described as

$${}^B\boldsymbol{x} = T_A^B({}^A\boldsymbol{x}) = {}^B\boldsymbol{R}_A {}^A\boldsymbol{x} + {}^B\boldsymbol{t}_A. \quad (1)$$

Let $\boldsymbol{p} = [\ X \ f]^T \in \Re^{6 \times 1}$ represents the generalized pose vector of the end effector in C_W , where $\boldsymbol{X} = [\ x \ y \ z]^T$ represents the position of the end effector in C_W , and $\boldsymbol{f} = [\ f_x \ f_y \ f_z]^T$ is a rotation vector that represents the orientation of C_E in C_W . The velocity of the

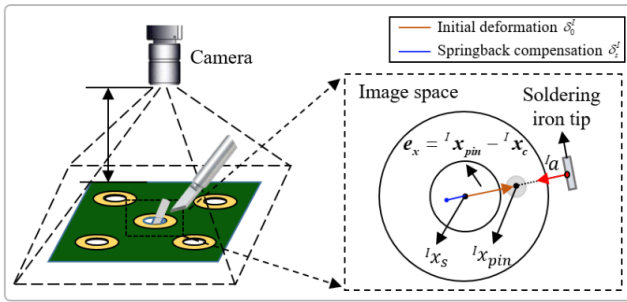


Fig. 4. The schematic of image-based pin alignment.

end effector in Cartesian space and the velocity in joint space is related using the Jacobian matrix as

$$\dot{\mathbf{p}} = \begin{bmatrix} \dot{\mathbf{X}} \\ \dot{\mathbf{f}} \end{bmatrix} = \mathbf{J}_p(\mathbf{q})\dot{\mathbf{q}}, \quad (2)$$

where $\mathbf{J}_p(\mathbf{q}) \in \mathbb{R}^{6 \times n}$ is the robot Jacobian matrix in word coordinate system,

$$\mathbf{J}_p(\mathbf{q}) = \begin{bmatrix} \mathbf{R}_E & \mathbf{0}_{3 \times 3} \\ \mathbf{0}_{3 \times 3} & \mathbf{R}_E \end{bmatrix} {}^E\mathbf{J}_p(\mathbf{q}), \quad (3)$$

where $\mathbf{R}_E \in \mathbb{R}^{3 \times 3}$ is orientation of C_E in world coordinate C , and ${}^E\mathbf{J}_p(\mathbf{q}) \in \mathbb{R}^{6 \times n}$ is the robot Jacobian matrix, representing the transmission ratio of velocity in joint space to velocity in Cartesian space.

Next, the dynamic model of the robot manipulator can be described by

$$\mathbf{M}(\mathbf{q})\ddot{\mathbf{q}} + \mathbf{C}(\dot{\mathbf{q}}, \mathbf{q})\dot{\mathbf{q}} + \mathbf{g}(\mathbf{q}) = \boldsymbol{\tau} \quad (4)$$

where $\boldsymbol{\tau} \in \mathbb{R}^n$ denotes the joint torque, which is the control input of the robot. The inertia $\mathbf{M}(\mathbf{q})$ is symmetric and positive definite, the matrix $\mathbf{M}(\mathbf{q}) - 2\mathbf{C}(\mathbf{q}, \dot{\mathbf{q}})$ is skew-symmetric.

Based on the pin-hole camera model, the coordinate transformation relationship between image coordinate system and world coordinate system is

$${}^I\mathbf{x} = \mathbf{T}_W^I(\mathbf{X}) = \frac{1}{\lambda(\mathbf{X})}\mathbf{K}^C (\mathbf{R}^C \mathbf{X} + \mathbf{t}^C), \quad (5)$$

where ${}^I\mathbf{x} \in \mathbb{R}^{2 \times 1}$ is the coordinate of a feature point in image space, $\mathbf{X} \in \mathbb{R}^{3 \times 1}$ is the three-dimensional coordinate of the feature point in C_W , $\mathbf{T}_W^I()$ is the transformation relationship from the word coordinate system to the image coordinate system, $\lambda(\mathbf{X})$ is the coefficient from homogeneous coordinate to Nonhomogeneous coordinate, $\mathbf{K}^C \in \mathbb{R}^{2 \times 3}$ is the internal parameter matrix of the camera, $\mathbf{R}^C \in \mathbb{R}^{3 \times 3}$ is the rotation matrix of camera in C_W , $\mathbf{t}^C \in \mathbb{R}^{3 \times 1}$ is the translation vector of the camera in C_W .

III. HIGH-PRECISION IMAGE-BASED PIN ALIGNMENT BY ROBOTIC MANIPULATION

For a pending solder joint, the camera provides the instantaneous image of the solder joint, and the image processing system extracts the information from the image for the design

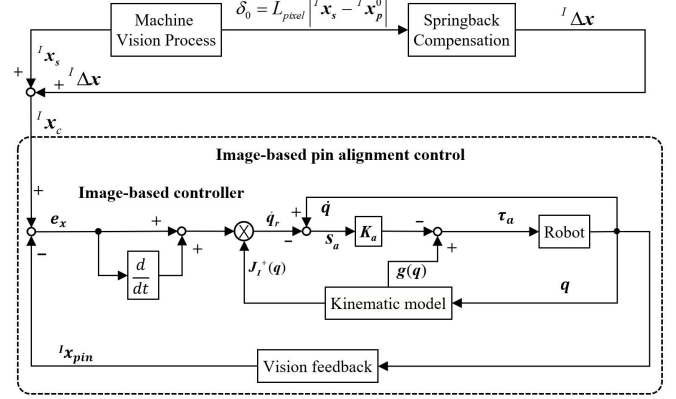


Fig. 5. Control scheme of the proposed precision image-based pin alignment controller.

of the controller. Then, the pin alignment is carried out by using the image-based visual servoing. The schematic of it is shown in Fig. 4, and the whole control scheme is shown in Fig. 5.

Firstly, a composite vector is proposed with considering the springback compensation

$${}^I\mathbf{x}_c = {}^I\mathbf{x}_s + {}^I\Delta x, \quad (6)$$

where ${}^I\mathbf{x}_s$ is the central position of the solder joint in image space, ${}^I\Delta x$ represents the springback displacement in image space, which can be calculated by

$${}^I\Delta x = \frac{B\left(L_{pixel} \left| {}^I\mathbf{x}_s {}^I\mathbf{x}_{pin}^0 \right|\right)}{L_{pixel}} \frac{{}^I\mathbf{x}_{pin}^0 {}^I\mathbf{x}_s}{{}^I\mathbf{x}_{pin}^0 {}^I\mathbf{x}_s}, \quad (7)$$

where L_{pixel} is the pixel equivalent of the camera, ${}^I\mathbf{x}_{pin}^0$ is the initial position of the pin's free end in image space, $B(\cdot)$ is the springback compensation function determined by enormous practical springback data. The pin is pushed to different positions by the manipulator from the same initial state, then the pin's springback displacement after unloading the external force is recorded. Each group of experiments is repeated 50 times, and the average value of each group of data is used to represent the springback data under this specific deformation state. Finally, those discrete data are used to fit the function $B(\cdot)$.

After determining the desired alignment stroke and direction, the high-precision pin alignment control can be completed under visual monitoring. The control term is proposed as

$$\boldsymbol{\tau}_a = -\mathbf{K}_a s_a + \mathbf{g}(q), \quad (8)$$

where \mathbf{K}_a is a positive-definite matrix, and s_a is a sliding vector proposed as

$$s_a = \dot{q} - \dot{q}_r, \quad (9)$$

where $\dot{q}_r = -\mathbf{J}_p^+(q)e_x + \mathbf{J}_p^+(q){}^I\dot{\mathbf{x}}_c$, $e_x = {}^I\mathbf{x}_{pin} - {}^I\mathbf{x}_c$, $\mathbf{J}_p^+(q)$ is the pseudo of $\mathbf{J}_p(q)$.

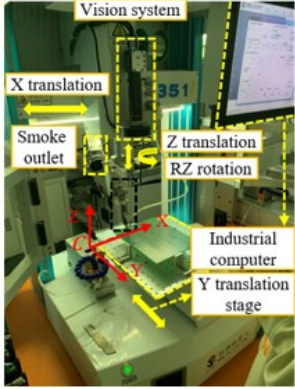


Fig. 6. A practical micromanipulation system configuration.

The dynamic model of the robot arm can be rewritten with the using of sliding vector as

$$\begin{aligned} M(\mathbf{q})(\ddot{\mathbf{q}} - \ddot{\mathbf{q}}_r + \ddot{\mathbf{q}}_r) + C(\dot{\mathbf{q}}, \mathbf{q})(\dot{\mathbf{q}} - \dot{\mathbf{q}}_r + \dot{\mathbf{q}}_r) + g(\mathbf{q}) = \\ M(\mathbf{q})\dot{\mathbf{s}}_a + C(\dot{\mathbf{q}}, \mathbf{q})\mathbf{s}_a + M(\mathbf{q})\ddot{\mathbf{q}}_r + C(\dot{\mathbf{q}}, \mathbf{q})\dot{\mathbf{q}}_r + g(\mathbf{q}) \\ = \boldsymbol{\tau} \end{aligned} \quad (10)$$

Substituting the controller $\boldsymbol{\tau}_a$, we have

$$M(\mathbf{q})\dot{\mathbf{s}}_a + (C(\dot{\mathbf{q}}, \mathbf{q}) + \mathbf{K}_a)\mathbf{s}_a = 0. \quad (11)$$

To carry out the stability analysis, a Lyapunov-like function is proposed as

$$V = \frac{1}{2}\mathbf{s}_a^T M(\mathbf{q})\mathbf{s}_a. \quad (12)$$

Differentiating V with respect to time yields

$$\dot{V} = \mathbf{s}_a^T M(\mathbf{q})\dot{\mathbf{s}}_a + \frac{1}{2}\mathbf{s}_a^T \dot{M}(\mathbf{q})\mathbf{s}_a. \quad (13)$$

Substituting the closed-loop equations (11) into (13) yields

$$\begin{aligned} \dot{V} &= -\mathbf{s}_a^T [C(\dot{\mathbf{q}}, \mathbf{q}) + \mathbf{K}_a]\mathbf{s}_a + \frac{1}{2}\mathbf{s}_a^T \dot{M}(\mathbf{q})\mathbf{s}_a \\ &= -\mathbf{s}_a^T \mathbf{K}_a \mathbf{s}_a + \frac{1}{2}\mathbf{s}_a^T [\dot{M}(\mathbf{q}) - 2C(\dot{\mathbf{q}}, \mathbf{q})] \\ &= -\mathbf{s}_a^T \mathbf{K}_a \mathbf{s}_a \leq 0. \end{aligned} \quad (14)$$

Since $V \geq 0$ and $\dot{V} \leq 0$, V is bounded. The boundedness of V ensures the boundedness of \mathbf{s}_a since $M(\mathbf{q})$ is bounded. According to classical theory, $\mathbf{s}_a \rightarrow 0$ as $t \rightarrow \infty$. In addition, since $\mathbf{J}_p(\mathbf{q})\mathbf{s}_a = \dot{\mathbf{x}} + \mathbf{e}_x$, the convergence of $\mathbf{s}_a \rightarrow 0$ means $\mathbf{e}_x \rightarrow 0$, which also indicates that ${}^I\mathbf{x}_{pin} \rightarrow {}^I\mathbf{x}_c$.

IV. EXPERIMENT

The proposed precise pin alignment method was verified in the practical microrobotic soldering system shown in Fig. 6. A digital microscope (AM4115TL, Dino-Lite Inc) with adjustable magnification (10X-140X) is used to provide visual feedback which has a resolution of 1080*960 and a frame rate of 30 fps. The robot has a manipulator with three active degrees of freedom (two translational and one rotational) and a passive degree of freedom as shown in Fig. 6. And there is also a translational fixture stage for moving the target into the operable area. The robot Jacobian matrix

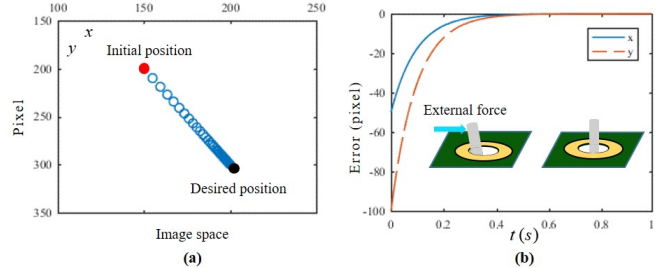


Fig. 7. Simulation results of image-based pin alignment controller. (a) The position trajectory of the end effector in image space. (b) Position error of the pin in image space.

${}^E\mathbf{J}_p(\mathbf{q})$ can be calculated by robot kinematics

$${}^E\mathbf{J}_p(\mathbf{q}) = \begin{bmatrix} -\cos \beta \sin \theta & \cos \beta \cos \theta & -\sin \beta & 0 \\ -\cos \theta & -\sin \theta & 0 & 0 \\ -\sin \beta \sin \theta & \sin \beta \cos \theta & \cos \beta & 0 \\ 0 & 0 & 0 & -\sin \beta \\ 0 & 0 & 0 & 0 \\ 0 & 0 & 0 & \cos \beta \end{bmatrix} \quad (15)$$

where β is the angle between the axis of the end actuator and the vertical direction, θ is the rotation angle of the rotation joint. And \mathbf{R}_E , the orientation of C_E in world coordinate C , is

$$\mathbf{R}_E = \begin{bmatrix} \cos \beta \cos \theta & -\sin \theta & \sin \beta \cos \theta \\ -\cos \beta \sin \theta & -\cos \theta & -\sin \beta \sin \theta \\ \sin \beta & 0 & -\cos \beta \end{bmatrix}. \quad (16)$$

Then the velocity of the end effector in the word coordinate system and the velocity in joint space can be related by

$$\mathbf{J}_p(\mathbf{q}) = \begin{bmatrix} \mathbf{R}_E & \mathbf{0}_{3 \times 3} \\ \mathbf{0}_{3 \times 3} & \mathbf{R}_E \end{bmatrix} = \begin{bmatrix} 0 & 1 & 0 & 0 \\ 1 & 0 & 0 & 0 \\ 0 & 0 & -1 & 0 \\ 0 & 0 & 0 & 0 \\ 0 & 0 & 0 & 0 \\ 0 & 0 & 0 & -1 \end{bmatrix}, \quad (17)$$

where we can see that the dimension of the row space of $\mathbf{J}_p(\mathbf{q})$ is 4, which means the rotation freedom of the end effector is restricted because of the insufficient degrees of freedom of rotation. And the first three columns of $\mathbf{J}_p(\mathbf{q})$ are orthogonal, which means the three translational degrees of freedom are decoupled.

A. Simulation Results

Before the experiment, the simulation initially proceeds to verify the performance of the proposed image-based visual servoing controller. The simulation is carried out in Matlab (2016a) of a PC with an Intel(R) Core(TM) i5-4210U CPU @ 2.4GHz processor and 4 GB RAM. The center of the pending solder joint in image space is set as (300, 300), and the initial position of the pin in image space is set as (200, 200). Fig. 7 shows the position error of the pin's free end in image space during the pin alignment control. It validates

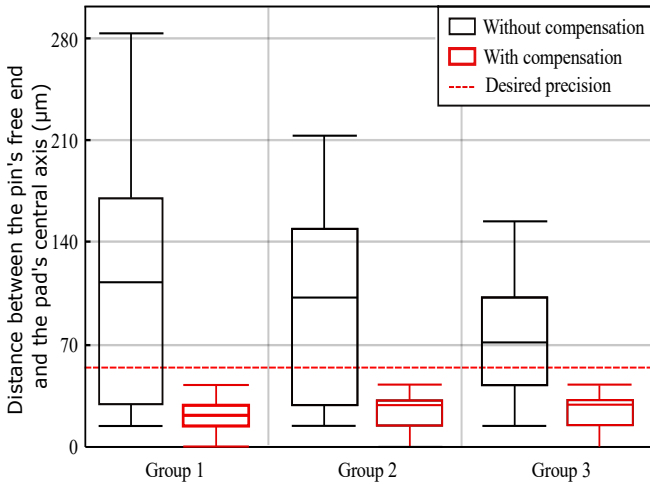


Fig. 8. Performance of pin alignment with and without springback compensation. Each group contains 20 solder joints with random initial pin offset position. The results indicate that the proposed pin alignment method with springback compensation in this paper has the advantages in both accuracy and stability comparing with the method without springback compensation.

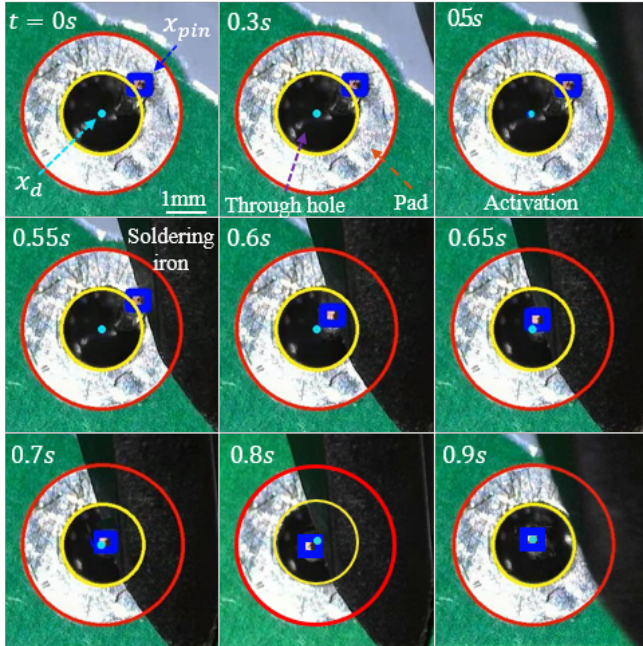


Fig. 9. A practical result of pin alignment with springback compensation.

that the image-based controller is feasible for moving the pin's free end to a desired position precisely. And it can be seen that the velocity of the end effector decreases gradually when it approaches the desired position, which ensures the pin can reach the desired position stably.

B. Experimental Results

Firstly, three groups of experiments are implemented by setting each group of 20 solder joints with random pin offset to validate the performance of the proposed pin alignment method. The comparison results (pin alignment with and without springback compensation) are shown in Fig. 8. It

clearly shows that the performance of pin alignment with springback compensation is much better, since the median and variance of errors in pin alignment with springback compensation are much smaller than that without springback compensation. In addition, the precision of pin alignment with springback compensation is approximately $30 \mu\text{m}$, which meets the precision requirement. To show how pin alignment with springback compensation works, Fig. 9 shows a practical result in image space. The pin's free end is moved beyond the central axis of the solder joint with springback compensation. Finally, the end effector is back to the heating position and the pin is back to the central axis of the solder joint due to its elastic recovery. And the movement speed of the pin's free end is inversely proportional to its distance from the desired position, which is consistent with the simulation results and can ensure the pin reach the desired position steadily. Fig. 10 also shows the result of automatic soldering with our proposed pin alignment operation, and it can be seen that the pin's free end is moved from the outside of the solder joint to the center of the solder joint by the manipulator.

V. CONCLUSION

This paper focuses on a problem to be solved in the electronic industry, that is, using robot operation to carry out high-precision pin alignment to improve the soldering quality. This research provides a solution for other robotic manipulation issues with plastic deformation and elastic recovery. However, the springback compensation data used in this paper is collected by a large number of experiments, which is time-consuming and inefficient. In future work, we will analyze the elastic recovery of electronic metal pin in depth, and use the elastoplastic deformation theory to calculate the springback compensation instead of experimental measurement.

REFERENCES

- [1] Z. Zhang, X. Wang, J. Liu, C. Dai, and Y. Sun, "Robotic micromanipulation: Fundamentals and applications," *Annual Review of Control, Robotics, and Autonomous Systems*, vol. 2, no. 1, pp. 181–203, 2019. [Online]. Available: <https://doi.org/10.1146/annurev-control-053018-023755>
- [2] L. Yang, I. Paranalawithana, K. Youcef-Toumi, and U. Tan, "Confidence-based hybrid tracking to overcome visual tracking failures in calibration-less vision-guided micromanipulation," *IEEE Transactions on Automation Science and Engineering*, vol. 17, no. 1, pp. 524–536, 2020.
- [3] S. Liu, D. Xu, Y.-F. Li, F. Shen, and D.-P. Zhang, "Nanoliter fluid dispensing based on microscopic vision and laser range sensor," *IEEE Transactions on Industrial Electronics*, vol. 64, no. 2, pp. 1292–1302, 2016.
- [4] B. Tiwari, C. Clévy, and P. Lutz, "High-precision gluing tasks based on thick films of glue and a microrobotics approach," *IEEE Robotics and Automation Letters*, vol. 4, no. 4, pp. 4370–4377, 2019.
- [5] T. Inoue, G. De Magistris, A. Munawar, T. Yokoya, and R. Tachibana, "Deep reinforcement learning for high precision assembly tasks," in *2017 IEEE/RSJ International Conference on Intelligent Robots and Systems (IROS)*. IEEE, 2017, pp. 819–825.
- [6] D. Xing, Y. Lv, S. Liu, D. Xu, and F. Liu, "Efficient insertion of multiple objects parallel connected by passive compliant mechanisms in precision assembly," *IEEE Transactions on Industrial Informatics*, vol. 15, no. 9, pp. 4878–4887, 2019.

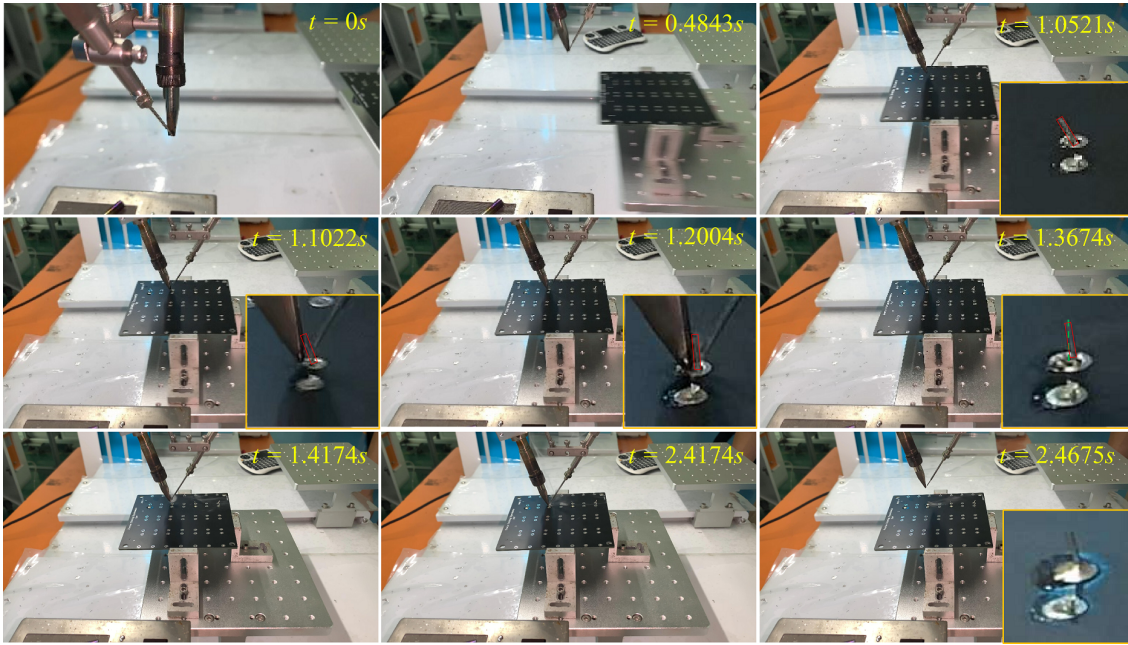


Fig. 10. A set of video frame sequences of experimental results of the proposed robotic micromanipulation method for precise soldering. The lower right corner of some video frames shows the local enlarged view of the solder joint to show the active pin alignment process, with the red box indicating the pin.

- [7] P. Wang, S. Shen, H. Lu, and Y. Shen, "Precise watch-hand alignment under disturbance condition by microrobotic system," *IEEE Transactions on Automation Science and Engineering*, vol. 16, no. 1, pp. 278–285, 2018.
- [8] Q. M. Ta and C. C. Cheah, "Stochastic control for orientation and transportation of microscopic objects using multiple optically driven robotic fingertips," *IEEE Transactions on Robotics*, vol. 35, no. 4, pp. 861–872, 2019.
- [9] C. Dai, Z. Zhang, Y. Lu, G. Shan, X. Wang, Q. Zhao, C. Ru, and Y. Sun, "Robotic manipulation of deformable cells for orientation control," *IEEE Transactions on Robotics*, 2019.
- [10] W. Shang, H. Ren, M. Zhu, T. Xu, and X. Wu, "Dual rotating microsphere using robotic feedforward compensation control of cooperative flexible micropipettes," *IEEE Transactions on Automation Science and Engineering*, 2020.
- [11] M. Yang, Y.-H. Ko, J. Bang, T.-S. Kim, C.-W. Lee, and M. Li, "Effects of ag addition on solid-state interfacial reactions between sn-ag-cu solder and cu substrate," *Materials Characterization*, vol. 124, pp. 250–259, 2017.
- [12] A. Mulugeta and S. Guna, "Lead-free solders in microelectronics," *Materials Science and Engineering: R: Reports*, vol. 27, no. 5-6, pp. 95–141, 2000.
- [13] D.-H. Jung, A. Sharma, and J.-P. Jung, "Influence of dual ceramic nanomaterials on the solderability and interfacial reactions between lead-free sn-ag-cu and a cu conductor," *Journal of Alloys and Compounds*, vol. 743, pp. 300–313, 2018.
- [14] C. L. S. C. Fonseka and J. A. K. S. Jayasinghe, "Implementation of an automatic optical inspection system for solder quality classification of tht solder joints," *IEEE Transactions on Components, Packaging and Manufacturing Technology*, vol. 9, no. 2, pp. 353–366, Feb 2019.
- [15] S. Hutchinson, G. D. Hager, and P. I. Corke, "A tutorial on visual servo control," *IEEE Transactions on Robotics and Automation*, vol. 12, no. 5, pp. 651–670, Oct 1996.